Efficient and expedited access to polyunsaturated fatty acids and biofunctional analogs by full solid-phase synthesis

Yutaro Saito,[1,†,*] Mayuko Akita,[1,†] Azusa Saika,[2,¶,†] Yusuke Sano,[1] Masashi Hotta,[2] Jumpei Morimoto,[1] Akiharu Uwamizu,[3] Junken Aoki,[3] Takahiro Nagatake,[2,‡] Jun Kunisawa,[2,4,5,6*] Shinsuke Sando[1,7*]

[1]Department of Chemistry and Biotechnology, Graduate School of Engineering, The University of Tokyo, 7-3-1 Hongo, Bunkyo-ku, Tokyo 113-8656, Japan

[2]Laboratory of Vaccine Materials and Laboratory of Gut Environmental System, Microbial Research Center for Health and Medicine, National Institutes of Biomedical Innovation, Health and Nutrition (NIBIOHN), 7-6-8 Asagi Saito, Ibaraki, Osaka 567-0085, Japan.

[3]Department of Health Chemistry, Graduate School of Pharmaceutical Sciences, The University of Tokyo, Bunkyo-ku, Tokyo, Japan.

[4]Department of Microbiology and Immunology, Kobe University Graduate School of Medicine, 7-5-1 Kusunoki-cho, Chuo-ku, Kobe, Hyogo 650-0017, Japan.

[5]International Research and Development Center for Mucosal Vaccines, The Institute of Medical Science, The University of Tokyo, 4-6-1 Shirokanedai, Minato-ku, Tokyo 108-8639, Japan.

[6]Graduate School of Medicine, Graduate School of Dentistry, Graduate School of Pharmaceutical Sciences, Department of Science, Osaka University, 1-1 Yamadaoka, Suita, Osaka 565-0871, Japan.

[7]Department of Bioengineering, Graduate School of Engineering, The University of Tokyo, 7-3-1 Hongo, Bunkyo-ku, Tokyo 113-8656, Japan.

[†] These authors contributed equally to this work.

[¶]Present address: Institute of Molecular and Cell Biology, Agency for Science Technology and Research, 11 Biopolis Way, #01-02, Helios, Singapore 138667, Singapore.

[‡] Present address: Laboratory of Functional Anatomy, Department of Life Sciences, School of Agriculture, Meiji University, 1-1-1 Higashi-Mita, Tama, Kawasaki, Kanagawa 214-8571, Japan.

***Contact corresponding authors**

Dr. Yutaro Saito

Department of Chemistry and Biotechnology, Graduate School of Engineering, The University of Tokyo

7-3-1 Hongo, Bunkyo-ku, Tokyo 113-8656, Japan

Email: saito.y@chembio.t.u-tokyo.ac.jp

ORCID: 0000-0001-7610-121X

Prof. Dr. Jun Kunisawa
Laboratory of Vaccine Materials and Laboratory of Gut Environmental System, Microbial Research Center for Health and Medicine, National Institutes of Biomedical Innovation, Health and Nutrition (NIBIOHN)
7-6-8 Asagi Saito, Ibaraki, Osaka 567-0085, Japan.
Email: kunisawa@nibiohn.go.jp
ORCID: 0000-0003-4901-1125

Prof. Dr. Shinsuke Sando
Department of Chemistry and Biotechnology, Graduate School of Engineering, The University of Tokyo
7-3-1 Hongo, Bunkyo-ku, Tokyo 113-8656, Japan
Email: ssando@chembio.t.u-tokyo.ac.jp
ORCID: 0000-0003-0275-7237

Abstract

Polyunsaturated fatty acids (PUFAs) represent a fundamental and essential lipid class, exhibiting versatile biofunctions. Lipidomic analysis has identified a growing number of lipid species, including PUFAs with diverse structural variations and biofunctions, yet the structure–function relationships are still largely unknown. In this context, there is a long-sought demand to synthesize various PUFAs efficiently. However, no practical methodology exists, unlike the case with peptides and nucleic acids, where diverse molecules are accessible through a well-established solid-phase synthesis. Herein, we report an efficient and expedited method to access a wide array of PUFAs by full solid-phase synthesis. This method allows the synthesis of various PUFAs and analogs in rapid and facile operations. Moreover, we have discovered an artificial fatty acid, *Antiefin*, with a high anti-inflammatory effect *in vivo* within our PUFA library. This report provides a practical synthetic pathway for PUFAs, a crucial lipid class, expected to contribute to lipid science.

Polyunsaturated fatty acid (PUFA), which is carboxylic acid with multiple unsaturated carbon–carbon bonds, is one of the pivotal lipid classes.[1,2] PUFAs exhibit various biological functions, either independently or as constituents of complex lipids. This lipid category involves numerous molecular species based on nuanced structural variations, thereby exhibiting diverse functions and properties (Fig. 1a). For example, eicosapentaenoic acid (EPA, **1a**) and docosahexaenoic acid (DHA, **1b**), both categorized as ω-3 fatty acids, have similar structures but play distinct physiological roles such as regulation of leukocyte functions and apoptosis signaling.[3] Arachidonic acid (ARA, **1c**), a representative ω-6 fatty acid, serves pro-inflammatory lipid mediators, in contrast to the ω-3 PUFAs could be converted into pro-resolving lipid mediators.[4–7] Mead acid (**1d**) is an ω-9 fatty acid recognized as an indicator for deficiency of the above essential fatty acids yet its detailed function is under elucidation.[8] Moreover, with the recent advancement of lipidomic technology, a growing number of functional PUFA metabolites have been discovered.[9] For example, 17,18-EpETE (**1e**) has been identified as an anti-inflammatory metabolite derived from **1a** through epoxidation by cytochrome P450 (CYP).[10,11] Given that **1a** does not exhibit the anti-inflammatory effect, the small structural difference between **1a** and **1e**, only one oxygen atom, is crucial for this effect. As exemplified, even subtle structural differences strongly affect the functions of PUFAs. Thus, a synthetic method for providing PUFAs with various fine-tuned structures is demanded to unveil their biofunctions, structure-property relationships, and mechanisms related to PUFAs.

Historically, the chemical synthesis of PUFAs has predominantly employed classical total synthesis in liquid-phase. These approaches often require highly specialized techniques for synthesizing and purifying unstable intermediates over a number of steps, making the process extremely time-consuming and labor-intensive.[12–14]

To tackle this limitation, we have adopted solid-phase synthesis. Solid-phase synthesis is a powerful

method for efficient synthesis and library construction of bioactive compounds.[15] Since its development by Merrifield in 1963,[16] this method has been utilized to synthesize a wide range of bioactive molecules contributing to combinatorial chemistry, chemical biology, and medicinal chemistry. Especially, this technique is widely used for the synthesis of biopolymers, including peptides, nucleic acids, and glycans. In this process, a molecular chain is chemically elongated on solid support by soaking and shaking the substrate-bound resin in a reaction solution. Following the reaction, the solution containing excess reagents and byproducts is easily removed by filtration and washing. Because these operations are much more facile compared with common liquid-phase synthesis, diverse sequences are easily accessed with appropriate coupling reactions and interchangeable building blocks in an iterative manner.[15] We envisioned that solid-phase synthesis enables access to structurally diversified PUFAs, as well as peptides, nucleic acids and glycans.

To this end, a significant challenge in synthetic organic chemistry should be addressed. Peptides, nucleic acids, and glycans are polymers or oligomers composed of amino acids, nucleotides, and monosaccharides, respectively. In addition, these monomers are linked by amide, phosphodiester, and glycoside bonds, which are relatively easy to form and cleave. By contrast, PUFAs present a different case. They do not possess such monomer units and linking bonds; the molecular structures consist of carbon–carbon bonds, which are generally difficult to form and cleave chemically. These fundamental differences underscore the challenge in synthesizing PUFAs compared to conventional biopolymers.

To achieve the solid-phase synthesis of PUFAs, it is first necessary to divide the PUFA structure into sequentially synthesizable units. Primarily, PUFA structure is composed of three parts: head moiety, including a carboxylic group and saturated chain; middle moiety, including methylene-interrupted *Z*-olefine structures; tail moiety, including a terminal alkyl chain (Fig. 1b, top). The chemical structures of

PUFAs are determined by the combination of the following three parameters: the carbon number of head moiety (δ), the olefine number of middle moiety (π), and the carbon number of tail moiety (ω). For example, the structure of EPA (**1a**) is expressed as [δ,π,ω] = [5,5,3]. Based on this structural feature, PUFA scaffolds can be constructed successively, with precise control of the δ, π, and ω (Fig. 1b, bottom). In our strategy, the head moiety (δ) is determined by loading carboxylic acids with the corresponding aliphatic chain lengths onto solid support. Subsequently, the middle moiety (π) is controlled by the iterative introduction of C3-allyl units with forming allylic or equivalent carbon–carbon bonds. Finally, the tail moiety (ω) is determined by utilizing the corresponding building blocks incorporated into PUFA chains in the final step of the chain elongation.

As a pioneering work, Janda and co-workers have reported the partial solid-phase synthesis of PUFAs and anandamide analogs in 2004 (Fig. 1c).[17] In the report, unsaturated fatty chains are elongated by constructing skipped alkyne structures *via* nucleophilic substitution between copper acetylides and propargyl halides.[13] This report suggests an important approach to achieve the PUFA synthesis on solid-phase. However, the method faces the following two challenges for a general and practical solid-phase synthesis (Fig. 1c). **Challenge (i)**: the elongation reaction suffers from inefficiency and requires lengthy time, leading to a highly time-consuming process (Elongation in Fig. 1c). For example, the synthesis of EPA (**1a**) involves four elongation reactions, taking 12 days (3 days × 4), even ignoring other incidental operations such as washing and drying resins. Furthermore, this synthesis requires about one more day for the reduction described below, resulting in a total of approximately 13 days for the entire process (Fig. 1e). **Challenge (ii)**: hydrogenation of poly-skipped alkynes, which are PUFA precursors, should be performed in liquid-phase after cleavage from resins; namely, this protocol is "partial" solid-phase synthesis (Reduction in Fig. 1c). In the hydrogenation process, poly-skipped alkynes, which are the most unstable intermediates during the synthesis, necessitate to be treated in liquid-phase.

Furthermore, the *Z*-selective reduction catalyzed by P-2 Ni, typical catalysis in liquid-phase, requires complicated procedures, including real-time monitoring and quenching at proper timing to avoid over-reduction.[12,13] These requirements cause difficulty in parallel synthesis. Therefore, it is essential to address these two **Challenges (i)** and **(ii)** to accomplish a general and practical solid-phase synthesis method of PUFAs.

Herein, we report the first "full" solid-phase synthesis of PUFAs overcoming the above challenges (Fig. 1d). The developed method allows efficient and expedited access to PUFAs that has not been possible by the previous methods in both liquid-phase and solid-phase. For example, the synthesis of EPA (**1a**) is completed within 6.5 h (except for incidental operations) while around 13 days by the previous methods (Fig. 1e). Moreover, this methodology has enabled us to construct a library containing a variety of PUFAs and has led to the discovery of a novel fatty acid, *Antiefin*, with very high anti-inflammatory effect *in cellulo* and *in vivo*.

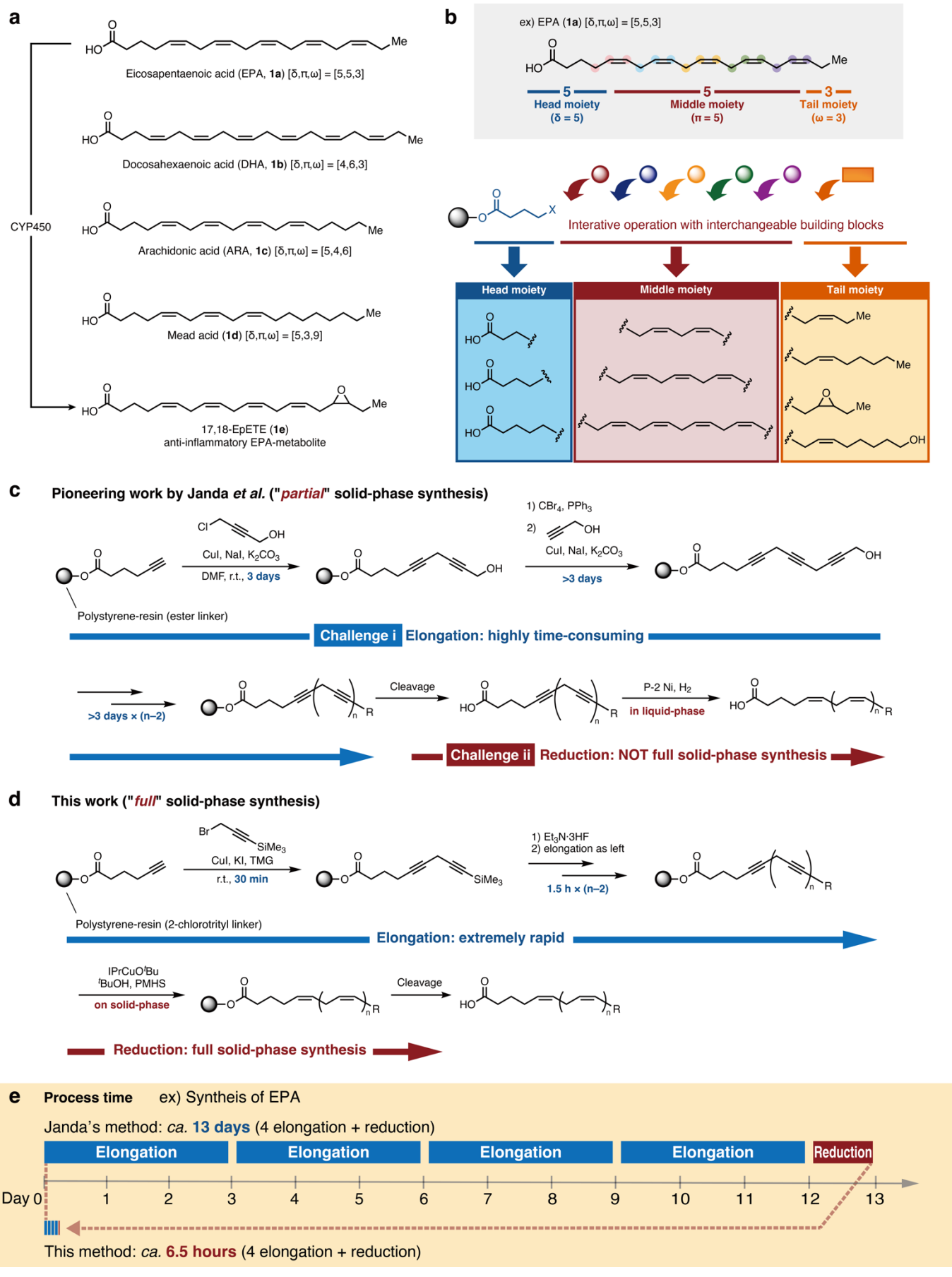

Fig. 1| Overview of this study. a, Representative PUFAs and metabolite. **b,** Chemical structure of PUFA and a synthetic strategy for diverse PUFAs on solid-phase. **c,** "Partial" solid-phase synthesis as a pioneering work by Janda *et al*.[17] **d,** This work: "full" solid-phase synthesis of PUFAs. TMG: 1,1,3,3-tetramethylguanidine, PMHS: polymethylhydrosiloxane. **e,** Comparison of time required in the previous and current methods.

Results and discussions

Selection of solid support

We selected polystyrene-based resin with 2-chlorotrityl linker as solid support in our synthesis. The previous report by Janda *et al*. used Wang-resin, polystyrene-based resin with benzyl ester linker, which requires strongly acidic conditions for cleavage.[17] Under such conditions, there is a concern of decomposition of products with some substituents including epoxides often found in PUFA metabolites.[18] In addition, intramolecular cyclization could occur to give undesired by-products when the PUFA on Wang-resin has a nucleophilic group.[17] This problem is solved by cleavage under mild conditions by employing the resin with the trityl-type linker. Indeed, 17,18-EpETE (**1e**) remained intact under the cleavage conditions for the resin with 2-chlorotrityl linker [30% 1,1,1,3,3,3-hexafluoroisopropanol (HFIP) in CH_2Cl_2] despite complete decomposition under the cleavage conditions for Wang-resin [50% trifluoroacetic acid (TFA) in CH_2Cl_2] (Supplementary fig. 1).

Overcoming the challenges toward solid-phase synthesis of PUFAs

We first attempted to improve the reaction efficiency in fatty chain elongation to overcome **Challenge (i)**. Shortening the reaction time in the elongation step was key because the previous method involved repeating the elongation reaction taking 3 days each (Elongation in Fig. 1c). We utilized 5-hexynoic acid conjugated with *tert*-butoxycarbonyl (Boc)-protected tryptophan [Trp(Boc)] on solid support **2** as a model substrate (Table 1, Top). Trp(Boc) moiety was employed for effective evaluation by HPLC analysis based on UV absorption at 280 nm, which is broadly used in peptide chemistry.[19] The elongation reaction of **2**

under the conventional conditions (4-chloro-2-butyn-1-ol as a coupling partner, K_2CO_3 as a base) was carried out with reaction time of 2 h (Table 1, entry 1). As consistent with the previous report,[17] the yield was low and the desired product was obtained in only 2%. We attributed this low efficiency to the low solubility of K_2CO_3 in the organic solvent. When this reaction is performed in liquid-phase, Na_2CO_3 or K_2CO_3 are usually utilized as bases to generate copper acetylide.[12–14] In the case of solid-phase, however, most of these inorganic bases exist as solids in organic solvents and cannot approach to terminal alkynes in polymer supports, resulting in the inefficient generation of copper acetylide. Based on this hypothesis, we explored bases with high solubility to promote the desired reaction. Cs_2CO_3, with higher solubility than K_2CO_3, improved the efficiency to 17% (Entry 2). Encouraged by this result, we further examined organic bases, which have higher solubility. Although a typical organic base Et_3N was not effective, a stronger and bulkier base $^{i}Pr_2NEt$ gave the desired product in 14% (Entries 3, 4). These results indicated that stronger and bulkier bases are preferred for this reaction. While 2,6-lutidine and 1,8-bis(dimethylamino)naphthalene (Proton Sponge®), which have low nucleophilicity, did not promote the reaction (Entries 5, 6), 1,8-diazabicyclo[5.4.0]undec-7-ene (DBU) afforded the desired product in 75% (Entry 7). Finally, 1,1,3,3-tetramethylguanidine (TMG) was found to accelerate the reaction dramatically to give excellent efficiency (>99%, Entry 8).

Table 1| Effect of base in the elongation reaction.

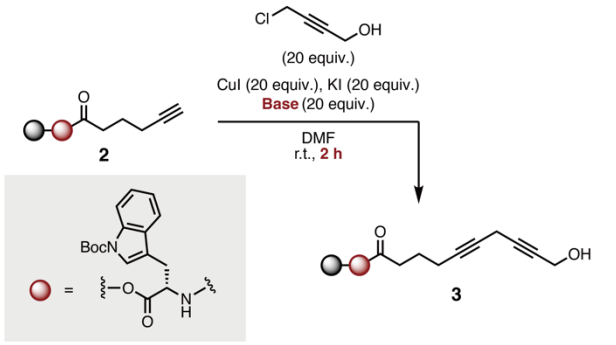

Entry	Base	HPLC ratio 3/(2+3)[a]	Entry	Base	HPLC ratio 3/(2+3)[a]
1	K_2CO_3	2%	5	2,6-lutidine	<1%
2	Cs_2CO_3	17%	6	Proton Sponge®	4%
3	Et_3N	<1%	7	DBU	75%
4	$^iPr_2NEt$	14%	8	TMG	>99%

[a]HPLC ratio was determined based on the ratio of HPLC peaks at 280 nm.

The resin-bound alcohol **3** obtained in the above reaction was converted into the propargyl bromide **4**, followed by the second elongation (Fig. 2a). However, the desired product **5** was obtained in only 4% yield even under the optimized conditions in Table 1 (Entry 8). We attributed this to the deactivation of the copper acetylide derived from propargyl alcohol as a coupling partner. In solid-phase synthesis, reactions are accelerated by increasing concentrations of reagents with excess amounts. Despite this advantage, copper acetylides are unavailable in this system because of deactivation by forming stable and insoluble assemblies in concentrated solutions.[20] Although several approaches have been suggested to circumvent this problem, such as activating the unreactive assemblies by umpolung[20] and disturbing the aggregation with bulky ligands[21], it is still hard to exploit copper acetylides in concentrated solutions. Indeed, yellow insoluble precipitation was generated immediately by mixing propargyl alcohol, CuI, and TMG in DMF (Fig. 2a). We concluded this phenomenon was the reason why the second elongation did not proceed.

In contrast to the second elongation, the initial elongation proceeded smoothly without producing precipitation as mentioned above (Table 1). The only difference between the first and second elongations lies in which of propargyl halide or copper acetylide exists on solid support. In the first elongation, copper acetylide on solid support reacts with propargyl halide in solution, while in the second elongation, propargyl halide on solid support reacts with copper acetylide in solution. Given that, the efficient reaction in the first elongation could have been achieved by the generation of copper acetylides on solid support, which isolates each molecule and suppresses the aggregation (Fig. 2b, bottom). Therefore, we adopted 3-(trimethylsilyl)propargyl bromide as an alternative coupling partner. After the elongation reaction, the terminal alkyne structure is re-generated by removing the terminal trimethylsilyl group, which enables iterative elongation by repeating the first elongation-type reaction and the deprotection (Fig. 2b). When the resin-bound 5-hexynoic acid **2′** was used as a substrate, the desired elongation proceeded efficiently in over 99% yield. Furthermore, the reaction was completed within only 30 min, probably because the leaving group was changed from chloride to bromide (Fig. 2b and Supplementary tables 1 and 2). For the deprotection reaction, $Et_3N{\cdot}3HF$[22] was employed to avoid generating undesired allenes by basic fluoride sources such as tetra-*n*-butylammonium fluoride (TBAF).[23] The terminal alkyne was obtained in 94% yield through the deprotection with $Et_3N{\cdot}3HF$ in DMF at room temperature under air for 1 h (Supplementary table 3). By implementing the optimized coupling reaction with 3-(trimethylsilyl)propargyl bromide (reaction time: 30 min) and deprotection (reaction time: 1 h), we succeeded in significantly accelerating the elongation of fatty chains, compared to the previous method. Furthermore, the present manner enables elongation by iterative operation of the coupling reaction and deprotection, similar to solid-phase peptide synthesis. By establishing this process, we overcame **Challenge (i)**.

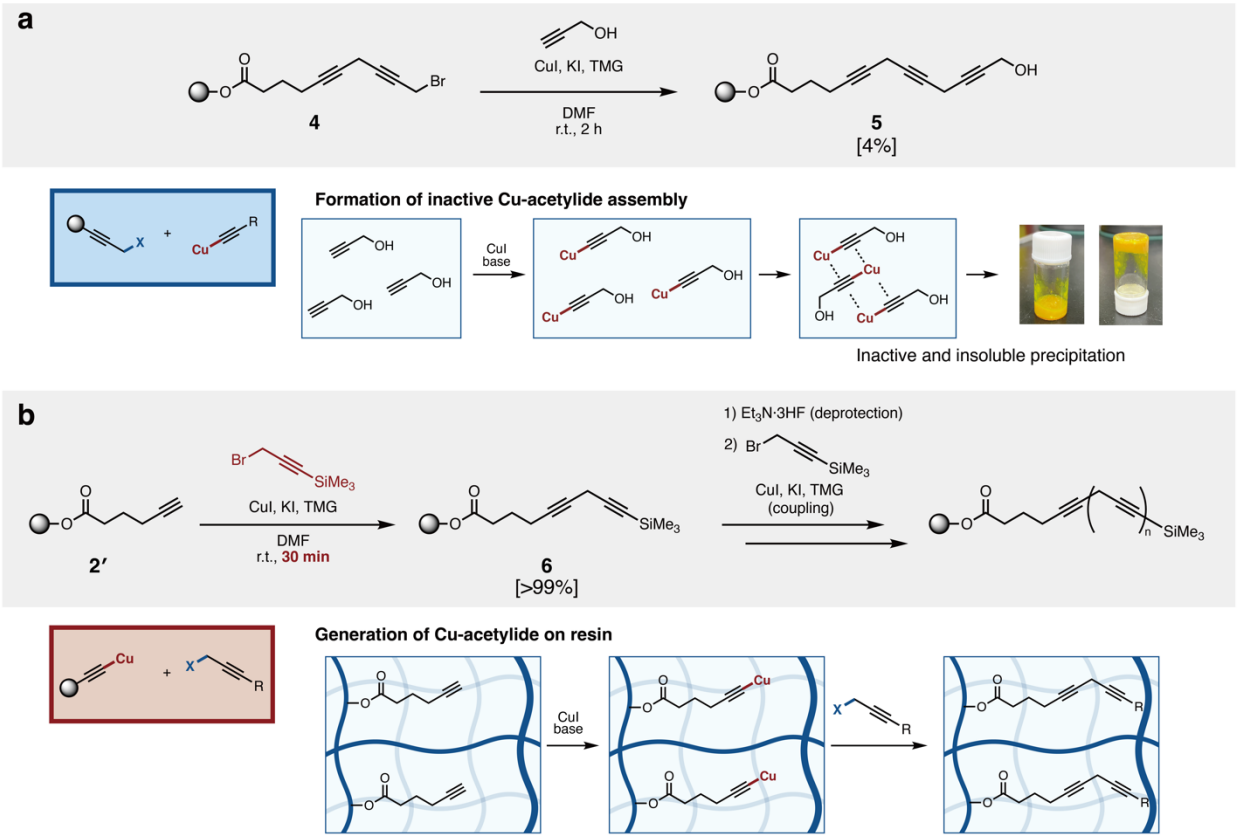

Fig. 2| Elongation reaction *via* copper acetylides in liquid-phase and on solid-phase. a, Elongation reaction *via* copper acetylide in liquid-phase. Reaction conditions: propargyl alcohol (18 equiv.), CuI (18 equiv.), KI (18 equiv.), TMG (18 equiv.), DMF, r.t., 2 h. The number in square brackets represents the yield determined by ^{1}H NMR. **b,** Elongation reaction *via* copper acetylide on solid-phase. Reaction conditions for the elongation: 3-(trimethylsilyl)propargyl bromide (20 equiv.), CuI (20 equiv.), KI (19 equiv.), TMG (20 equiv.), DMF, r.t., 30 min. Reaction conditions for the deprotection: $Et_3N{\cdot}3HF$ (20 equiv.), DMF, r.t., 1 h. The number in square brackets represents the yield determined by ^{1}H NMR.

To address **Challenge (ii)** and to accomplish "full" solid-phase synthesis of PUFAs, we explored semi-reduction system of alkynes on solid-phase. We considered that typical reduction systems in PUFA synthesis such as hydrogenation with Lindlar's catalyst[14] or P-2 Ni[12,13] are not suitable for the solid-phase synthesis because the reactions are heterogeneous, and the active catalysts are impossible to access the

inside of resins. Moreover, these reactions require real-time monitoring and quenching at proper timing to avoid over-reduction, leading to complicated operations. We then focused on the homogeneous catalysis reported by Lalic and a co-worker with a copper complex with an *N*-heterocyclic carbene ligand.[24] The semi-reduction by this catalysis is reported to proceed under mild conditions with high *Z*-selectivity without over-reduction. We further optimized the conditions for the reaction on solid-phase. The reduction of the model substrate **7** was evaluated by liquid chromatography-mass spectrometry (LCMS) (Table 2). The initial conditions [IPrCuO^{t}Bu 50 mol%, ^{t}BuOH 50 equiv., PMHS 70 equiv., 50 °C, 30 min; IPr = 1,3-bis(2,6-diisopropylphenyl)imidazol-2-ylidene] resulted in 26% yield of the desired product **8** (Entry 1). In this reaction, only the desired product **8**, intermediates with alkynes and alkenes, and a trace amount of the substrate **7** were observed except for subtle impurities (Supplementary fig. 2). Twice the amount of the reagents improved the yield to 91% (Entry 2). Further increase of ^{t}BuOH to 175 equiv. or decrease to 50 equiv. resulted in slightly decreased yields (Entries 3, 4). The yield was reduced to 31% by an additional increase of PHMS to 280 equiv. (Entry 5). The reaction under the best conditions of Entry 2 produced a high yield even when the reaction time was shortened to 20 min (84%, Entry 6) while the yield significantly decreased to 68% when the reaction time was 10 min (Entry 7). Through these investigations, we selected the conditions of Entry 6 (IPrCuO^{t}Bu 100 mol%, ^{t}BuOH 100 equiv., PMHS 140 equiv., 50 °C, 20 min) as the optimal conditions. Although the intermediates remain after this single reaction, the reduction can be completed by repeating because no over-reduction product was observed in this system. Indeed, the reduction was completed to afford >99% HPLC yield by performing this reaction twice without generating any by-products (Entry 8 and supplementary fig. 2). In solid-phase synthesis, such repeating operations can be conducted easily because reagents and by-products in solution can be removed just by filtration and washing. Through these investigations, we overcame **Challenge (ii)**.

Table 2| Semi-hydrogenation reaction of the skipped alkyne on solid-phase.

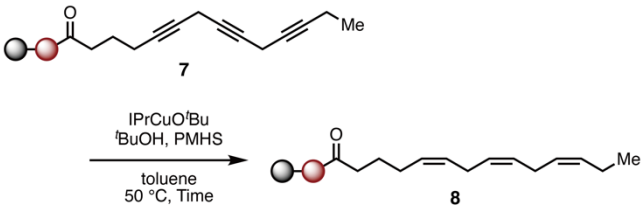

Entry	IPrCuO^{t}Bu	^{t}BuOH	PMHS	Time	HPLC yield[a]
1	50 mol%	50 equiv.	70 equiv.	30 min	26%
2	100 mol%	100 equiv.	140 equiv.	30 min	91%
3	100 mol%	175 equiv.	140 equiv.	30 min	76%
4	100 mol%	50 equiv.	140 equiv.	30 min	86%
5	100 mol%	50 equiv.	280 equiv.	30 min	31%
6	100 mol%	100 equiv.	140 equiv.	20 min	84%
7	100 mol%	100 equiv.	140 equiv.	10 min	68%
8[b]	100 mol%	100 equiv.	140 equiv.	20 min	>99%

[a]HPLC yield was determined based on the ratio of HPLC peaks at 280 nm. [b]The reaction was performed twice.

The developed protocol for solid-phase synthesis of PUFAs, overcoming **Challenges (i)** and **(ii)**, is summarized in Fig. 1d. With this optimized method in hand, we performed PUFA synthesis. As a representative example, the synthesis of Trp(Boc)-tagged EPA **10** is described in Fig. 3a. Trp(Boc)-tagged 5-hexynoic acid on polymer support **2** was subjected to the elongation to afford the skipped diyne **6′**. After deprotection with $Et_3N{\cdot}3HF$, the elongation reaction was performed again. These processes were repeated one more time, and the terminal moiety was introduced by utilizing 1-bromopent-2-yne, instead of 3-(trimethylsilyl)propargyl bromide, in the final coupling reaction to produce the PUFA precursor **9**. Trp(Boc)-EPA **10** was successfully obtained through the hydrogenation with IPrCuO^{t}Bu complex followed by cleavage under mild conditions (30% HFIP in CH_2Cl_2). HPLC analysis revealed that the starting material was consumed completely and the desired product **10** was obtained with high selectivity (80% purity analyzed by HPLC at 280 nm) (Fig. 3b). The developed protocol allowed efficient and

expedited synthesis of Trp(Boc)-EPA **10**. By addressing **Challenges (i)** and **(ii)**, a series of the synthesis was completed in 6.5 h (except for other incidental operations such as washing and drying resin). In the previous method, the synthesis is predicted to take about 13 days. Thus, the current protocol enables extremely rapid access to the target PUFAs (Fig. 1e). Furthermore, the simple and easy operations compared with liquid-phase syntheses allow parallel synthesis, which are useful for simultaneous synthesis of PUFAs with structural variations.

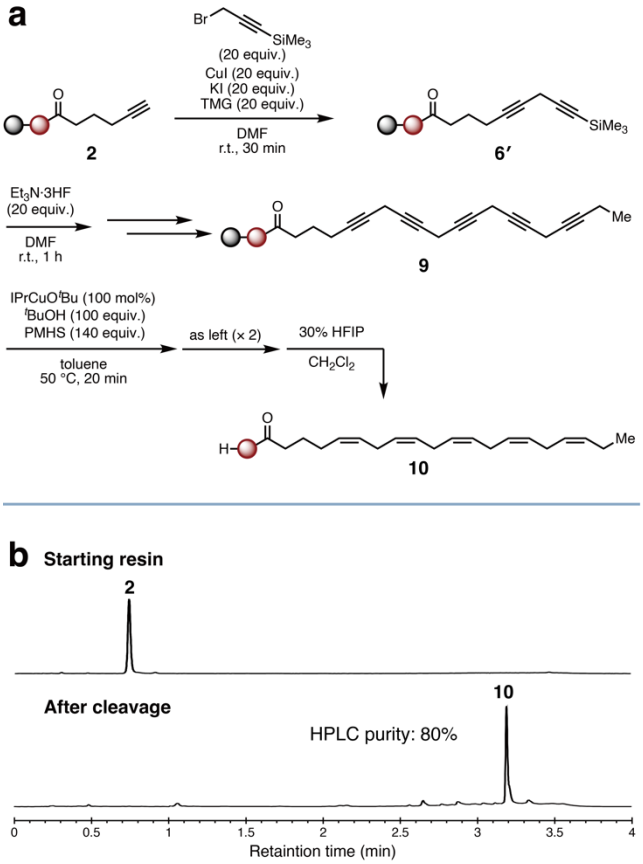

Fig. 3| Solid-phase synthesis of Trp(Boc)-tagged EPA 10. a, Synthetic scheme of Trp(Boc)-EPA **10**. **b,** HPLC analysis of the crude samples cleaved from the starting resin (top) and the resin after the synthetic process (bottom). UV absorption was monitored at 280 nm. HPLC purity was calculated based on the area ratio of peaks with intensities higher than 1% of the main peak.

Solid-phase synthesis of PUFAs and their derivatives

We synthesized various PUFAs and their derivatives with the developed protocol (Table 3). In all cases, the desired compound was the dominant component in the crude product after cleavage from the resin. No spot other than the desired product was observed in thin layer chromatography (TLC) analysis except for the baseline spot, and the target PUFAs were obtained through facile purification by silica-gel chromatography (total yields: 45–89%, HPLC purity: 75–99%). Purification by HPLC yielded pure PUFAs for biological assays.

By varying carboxylic acids loaded onto the resin and the repeating number of the elongation, ω-3 PUFAs **1a**, **1b**, and **1f**–**l** with different chain lengths and unsaturated structures (numbers and positions of olefines) were successfully synthesized (ω-3 series in Table 3). The PUFAs with the olefine number of four ($\pi = 4$) **1f**, **1h**, **1j** were obtained in around 80% yields over six steps from the starting materials (the first line in Table 3). The PUFAs with $\pi = 5$ **1a**, **1g**, **1k** were obtained in moderate yields (52–68% over eight steps, the second line in Table 3). The PUFAs with $\pi = 6$ **1b**, **1i**, **1l** were also obtained in sufficient yields (45–55% over ten steps, the third line in Table 3). Applying the responsible building blocks for the tail moiety enabled the synthesis of unnatural ω-2 PUFA **1m**, natural ω-6 PUFA **1c**, and ω-9 PUFA **1d** (various ω series in Table 3). These PUFAs were obtained in high yields (66–89%). Thus, the current method allowed precise control of the head, middle, and tail moieties in PUFA synthesis.

PUFA derivatives with functional groups at the terminal moieties were also successfully synthesized by employing the relevant building blocks (metabolites and rare PUFAs in Table 3). Oxylipins, oxidized PUFA metabolites with hydroxy and/or epoxy groups, are known as major bioactive metabolites.[5] As mentioned above, 17,18-EpETE (**1e**) is a functional metabolite derived from EPA (**1a**) through

epoxidation at C17,18-position catalyzed by CYPs.[25] Our solid-phase synthesis supplied **1e** successfully and its analog **1n** in 55% and 67% yields. Hydroxy fatty acids 20-HEPE (**1o**) and 20-HETE (**1p**) are also oxylipins derived from EPA (**1a**) and ARA (**1c**), respectively.[26–28] These hydroxy fatty acids were successfully obtained in 45% and 72% yields. No significant side-reactions such as epoxide ring-opening (Supplementary fig. 1) and intramolecular cyclization between hydroxy groups and the linker-ester group[17], which is problematic in the previous report, occurred during the process because this method does not include any reactions under strongly acidic conditions.

Rare fatty acids that occur naturally only in very small quantities can also be accessed by our method. Furanyl fatty acids are bioactive compounds found in plants, algae, and fish.[29] These fatty acids and their derivatives have been rarely investigated because of the severely limited supply from nature. We synthesized unreported furanyl PUFAs **1q** and **1r** in 59% and 87% yields, respectively. Our synthesis could contribute to biological investigation on such rare fatty acids, which are difficult to obtain enough amount from nature.

Table 3| Polyunsaturated fatty acids prepared through solid-phase synthesis.

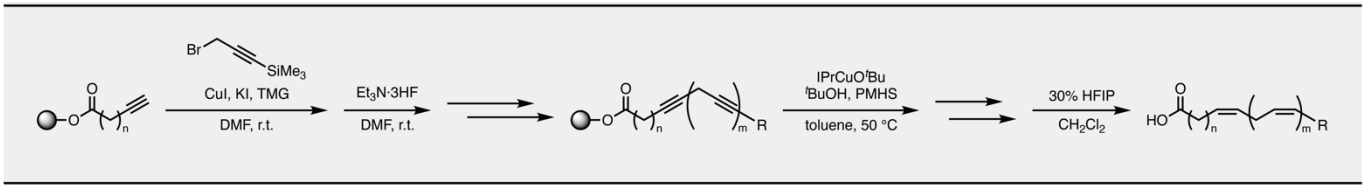

ω-3 series

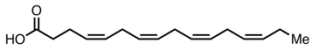

1f [δ,π,ω] = [4,4,3]
78%[a] (89%)[b]

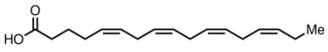

1h [δ,π,ω] = [5,4,3]
81%[a] (88%)[b]

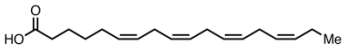

1j [δ,π,ω] = [6,4,3]
76%[a] (89%)[b]

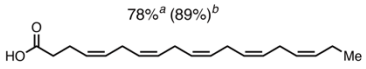

1g [δ,π,ω] = [4,5,3]
52%[a] (81%)[b]

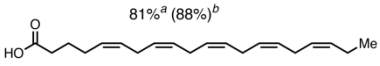

EPA (**1a**) [δ,π,ω] = [5,5,3]
63%[a] (85%)[b]

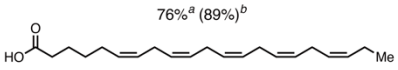

1k [δ,π,ω] = [6,5,3]
68%[a] (77%)[b]

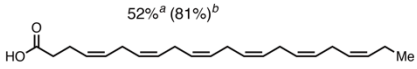

DHA (**1b**) [δ,π,ω] = [4,6,3]
45%[a] (77%)[b]

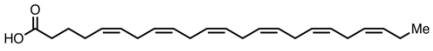

1i [δ,π,ω] = [5,6,3]
51%[a] (75%)[b]

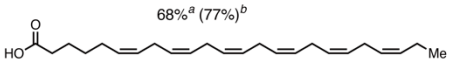

1l [δ,π,ω] = [6,6,3]
55%[a] (75%)[b]

Various ω series

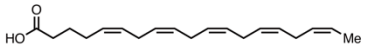

1m [δ,π,ω] = [5,5,2]
66%[a] (85%)[b]

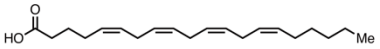

ARA (**1c**) [δ,π,ω] = [5,4,6]
70%[a] (86%)[b]

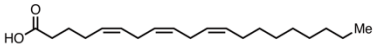

Mead acid (**1d**) [δ,π,ω] = [5,3,9]
89%[a] (94%)[b]

Metabolites and rare PUFAs

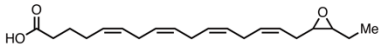

17,18-EpETE (**1e**)
55%[a] (91%)[b]

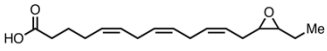

1n
67%[a] (97%)[b]

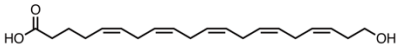

1o
45%[a] (90%)[b]

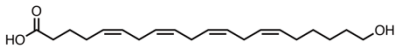

1p
72%[a] (90%)[b]

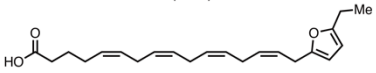

1q
59%[a] (84%)[b]

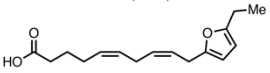

1r
87%[a] (99%)[b]

[a]Yield after purification by silica-gel column chromatography. [b]HPLC purity (at 210 nm) based on the area ratio of peaks with intensities higher than 1% of the main peak.

FFAR1 agonistic activity of PUFAs in the library

We evaluated agonistic activity for Free fatty acid receptor 1 (FFAR1, GPR40) with the constructed PUFA library in Table 3. FFAR1 is a G protein-coupled receptor (GPCR) known to be activated by a wide range of middle- and long-chain fatty acids, particularly by PUFAs and their metabolites.[11,27,30,31] This receptor has attracted attention as a therapeutic target for inflammatory pain, central nervous system diseases, and diabetes.[31–33] Despite vigorous investigation on agonistic activities of naturally abundant

PUFAs[30] and the development of artificial synthetic agonists[33], unnatural or rare PUFAs and their metabolites have rarely been investigated.

In this context, we evaluated FFAR1 agonistic activities of PUFAs described in Table 3 by TGFα shedding assay.[34] In this assay, GPCR activation is detected from the shedding of alkaline phosphatase (AP)-tagged transforming growth factor-α (TGFα) mediated by tumor necrosis factor α-converting enzyme (TACE) (Fig. 4a). We investigated FFAR1 agonistic activity of each PUFA in the library at 3.0 μM (Fig. 4b). Among ω-3 PUFAs (**1a**, **1b**, and **1f**–**l**), the shortest PUFA **1f** ([δ,π,ω] = [4,4,3]) exhibited the highest agonistic activity. This finding is consistent with the previous report that **1f** activates FFAR1,[35] and is interesting in terms of the activity higher than those of naturally abundant ω-3 PUFAs such as EPA (**1a**) and DHA (**1b**). The agonistic activity of the uncommon ω-2 PUFA **1m** [5,5,2] was slightly higher than that of ω-3 EPA (**1a**), ω-6 ARA (**1c**), and ω-9 mead acid (**1d**), indicating that only a slight difference in ω-moiety alters FFAR1 activation. The epoxy metabolite 17,18-EpETE (**1e**), known as an FFAR1 agonist,[11] exhibited high agonistic activity. Another epoxy analog **1n**, with one less double bond, possessed low activity, indicating that the olefine number and/or chain length are crucial for FFAR1 activation by **1e**. The FFAR1 agonistic activity of 20-HEPE (**1o**) has not been reported while 20-HETE (**1p**), with an ω-hydroxy group as well as **1o**, has attracted attention due to its anti-diabetic activity through FFAR1 activation.[27] In our assay, the agonistic activity of **1o** was higher than that of **1p**, offering a potential of **1o** as therapeutic material as well as **1p**. Although the ω-hydroxy group contributes to enhancing the FFAR1 agonistic activity (vs. their precursors **1a** and **1c**), FFAR1 may recognize not only the hydroxy group but also the other structural properties because the agonistic activities of **1o** and **1p** are different. Interestingly, the furanyl fatty acid **1r** also displayed high agonistic activity.

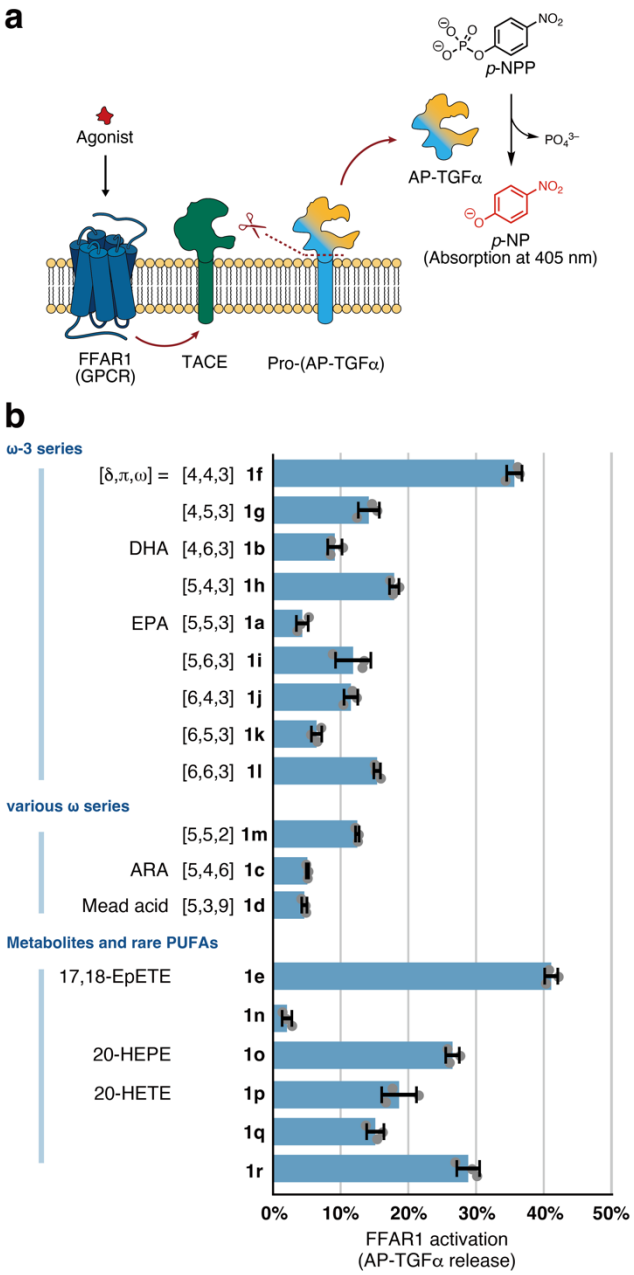

Fig. 4| FFAR1 activation by the synthesized PUFAs in TGFα shedding assay. a, Schematic illustration of TGFα shedding assay. TACE: tumor necrosis factor α-converting enzyme (ADAM17), AP: alkaline phosphatase, TGFα: transforming growth factor-α, *p*-NPP: *para*-nitorophenylphosphate, *p*-NP: *para*-nitrophenol. **b,** FFAR1 agonistic activation by PUFAs **1a**–**1r**. Concentration of PUFAs: 3.0 μM. Error bars indicate the SD, $n = 3$.

Development of a novel fatty acid exerting the anti-inflammatory effect *in vivo*

As mentioned above, FFAR1 agonist is promising to display various therapeutic effects.[31–33] For example, the epoxy fatty acid **1e,** metabolically produced from **1a**, is an FFAR1 agonist and known to be a potential anti-inflammatory PUFA metabolite. It inhibits Rac activation through FFAR1-mediated signaling in neutrophils, resulting in preventing neutrophil migration *via* suppression of pseudopod formation, leading to an anti-inflammatory effect.[11] However, **1e** lost this effect upon conversion into 17,18-diHETE (**1s**) by soluble epoxide hydrolase (sEH) *in vivo* (Fig. 5a).[11,36] Therefore, a bio-stable isostere of **1e** with an anti-inflammatory effect in the same mechanism is beneficial in terms of pharmaceutical development and mechanism investigation.

We focused on the furanyl fatty acid **1r**, considering the result of TGFα shedding assay in Fig. 4. This molecule possesses high FFAR1 activity (Fig. 4b) and is predicted to tolerate metabolism by sEH due to the absence of the epoxy group. We expected **1r** to be a bioisostere of **1e** with biostability (Fig. 5a). As an initial test, we evaluated the stability of **1e** and **1r** in mouse liver homogenate where sEH is highly expressed (Fig. 5b).[37,38] While a large amount of **1e** was degraded after one-hour incubation, **1r** remained almost intact. Given that the consumption of **1e** was inhibited completely in the presence of *N*-[1-(1-oxopropyl)-4-piperidinyl]-*N*′-[4-(trifluoromethoxy)phenyl]urea (TPPU)[39,40], an sEH inhibitor, the major metabolism of **1e** in liver is attributed to sEH and that **1r** successfully circumvents this degradation. This result indicated that **1r** has the potential to work *in vivo* as a stabilized bioisostere of **1e**.

Next, **1r** was investigated on the inhibition ability against neutrophil pseudopod formation *in vitro* (Figs. 5c and 5d).[11,41] Purified neutrophils from mouse bone marrow were treated with **1e**, **1r**, or EtOH (vehicle), followed by stimulation with leukotriene B_4 (LTB_4) to induce pseudopod formation. After cell

fixation, the degree of pseudopod formation was evaluated by F-actin staining. The furanyl fatty acid **1r** exhibited an obvious inhibitory effect at 100 nM as well as **1e**. Notably, **1r** strongly prevented the pseudopod formation even at an extremely low concentration (0.1 nM) while such an effect was observed in the case of **1e** only at above 100 nM.

Finally, the anti-inflammatory effect of **1r** was tested in *in vivo* experiments using contact hypersensitivity model mice (Figs. 5e–h).[11] Mice were treated with **1e**, **1r**, or EtOH (vehicle) followed by sensitization with 2,4-dinitrofluorobenzene (DNFB). After five days, the mice were treated again with the corresponding PUFA 30 min before inflammation induction with DNFB at the fronts and backs of both ears. At 48 h after DNFB stimulation, ear thickness (Fig. 5f) and neutrophil accumulation in the ear (Fig. 5g) were measured. Ear swelling and neutrophil accumulation of mice treated with 100 ng of **1e** or **1r** were significantly suppressed compared with those of mice treated with a vehicle. Moreover, **1r** exhibited a significant anti-inflammatory effect in the case of 10 ng although the effect was not observed in the case of 10 ng of **1e** (Figs. 5f–h). This result demonstrated that **1r** is a promising analog with a high anti-inflammatory effect *in vivo*.

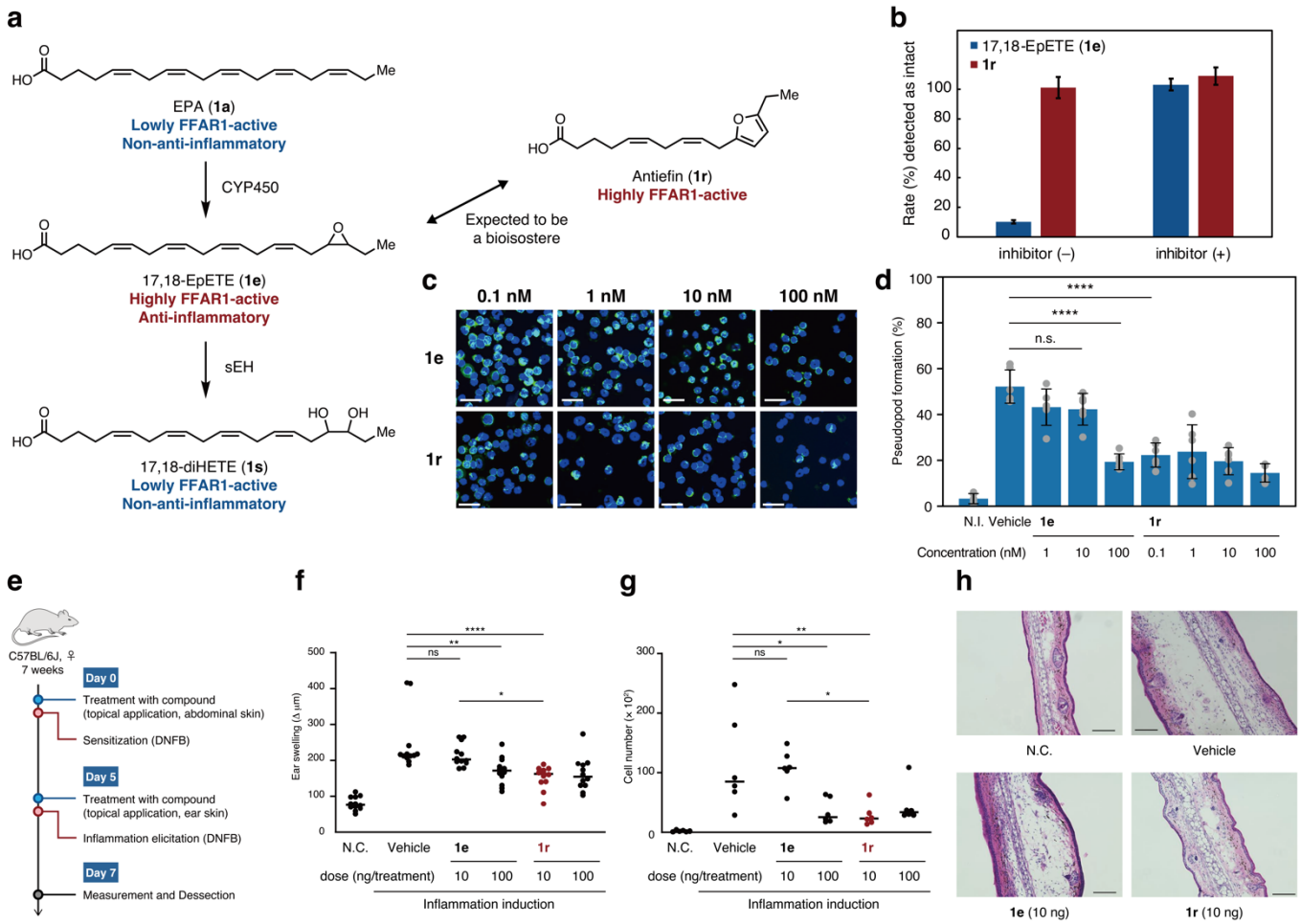

Fig. 5| Anti-inflammatory effect of the furanyl PUFA 1r. a, Metabolic pathway related with 17,18-EpETE (**1e**) and furanyl fatty acid **1r**. **b,** Metabolic tolerance of **1e** and **1r** in mouse liver homogenate in the absence or presence of an sEH inhibitor, TPPU. The compounds were incubated in mouse liver homogenate at 37 °C for 1 h. For the reaction with the inhibitor, the liver homogenate was pre-incubated in the presence of 200 μM TPPU at 37 °C for 15 min. The residual amount of each compound was analyzed by LCMS. **c,** Images of inhibition against pseudopod formation of neutrophils by **1e** and **1r**. Neutrophil pseudopod was stained with phalloidin. Neutrophils were treated with either **1e** or **1r** for 15 min before stimulation with LTB_4. The final concentrations of PUFA are shown at the top of each image. Green: phalloidin indicating the pseudopod formation, Blue: DAPI. Scale bars: 20 μm. **d**, Plots of inhibition against pseudopod formation of neutrophils by **1e** and **1r**. Bar graphs indicate averages of values obtained in six independent experiments. Error bars indicate the SD. ****P <0.0001. n.s.: not significant. N.I.: non LTB_4-induction control. **e–h,** Evaluation of anti-inflammatory effect *in vivo*. **e,** Schematic representation of the experimental outline. **f–g,** Plots of ear swelling and neutrophil accumulation. Mice were treated with either 17,18-EpETE (**1e**) (10 or 100 ng in DPBS), **1r** (10 or 100 ng in DPBS), or vehicle (50% EtOH in DPBS) by topical application on the abdominal skin; on Day 5, mice were then stimulated with DNFB 30 min after topical application with the corresponding PUFA or vehicle (the same dose of the Day 0) on the ear skin. Ear swelling (**f**)

and numbers of neutrophils in the ear (**g**) were evaluated on Day 7. Data are combined from three independent experiments, and each point represents data from an individual mouse. Center values indicate medians. Statistical significance was evaluated by using one-way analysis of variance with post-hoc Tukey test for multiple comparisons. N.C.: non-elicitation control group. *P <0.1, **P <0.01, and ****P <0.0001. n.s.: not significant. **h,** Representative microscope images of frozen mice-ear sections treated with **1e** or **1r** (10 ng/treatment) stained with hematoxylin and eosin. Scale bars: 100 μm.

Conclusion

We have developed the "full" solid-phase synthesis for precise and diverse synthesis of PUFAs. The present method allows for the efficient and expedited synthesis of various PUFAs with diverse structures regardless of whether the target PUFA is naturally derived or not. A wide range of PUFAs with different chain lengths and terminal structures are available in this system by utilizing proper building blocks.

Furthermore, we have successfully constructed the PUFA library, investigated FFAR1 agonistic activity, and discovered a novel analog with an anti-inflammatory effect *in vivo*. It should be noted that this newly discovered furanyl PUFA analog **1r** is more effective than the epoxy PUFA analog **1e** known for its anti-inflammatory effects, showing cellular anti-inflammatory activity, comparable to the epoxy PUFA analog **1e**, even at concentrations 1,000 times lower. We have named this biofunctional fatty acid **1r** *Antiefin* (anti-inflammatory ethylfuranyl fatty acid).

Our synthetic strategy not only provides rapid access to the target PUFAs but also facilitates the construction of large libraries, contributing to the discovery of PUFAs with unknown functions and the development of new chemical tools. Solid-phase synthesis has contributed to making great strides in the fields of peptide, nucleic acid, and glycan. Our method is expected to be a crucial milestone in linking solid-phase synthesis to advances in lipid science. Building on the foundations laid in this report, our group is going to establish efficient synthetic methodologies for unprecedented lipids and explore their biological applications.

Methods

General procedures for solid-phase synthesis of PUFAs (Table 3)

[Step 1: chain-elongation]

To a 6-mL plastic syringe equipped with a filter were added the corresponding resin conjugated with ethynyl carboxylic acid (20.0 μmol), CuI (76.2 mg, 400 μmol, 20 equiv.), and KI (66.4 mg, 400 μmol, 20 equiv.). The syringe was purged with N_2 through evacuation and filling back N_2 three times. To the syringe were added 3-(trimethylsilyl)propargyl bromide (65.3 μL, 400 μmol, 20 equiv.) and 1,1,3,3-tetramethylguanidine (TMG) (50.1 μL, 400 μmol, 20 equiv.) in DMF (1.0 mL). The syringe was shaken continuously for 30 min. After removing the reaction solution, the resin was washed with DMF (× 3).

[Step 2: deprotection]

To the vessel were added DMF (1.0 mL) and $Et_3N{\cdot}3HF$ (69.3 μL, 400 μmol, 20 equiv.). The syringe was shaken continuously for 1 h. After removing the reaction solution, the resin was washed with DMF (× 3), MeOH (× 3), and CH_2Cl_2 (× 3) and dried under reduced pressure.

Steps 1 and 2 were repeated until the desired chain length was obtained.

[Step 3: introduction of terminal moiety]

The elongation reaction of Step 1 was performed using the corresponding propargyl bromide instead of 3-(trimethylsilyl)propargyl bromide. After removing the reaction solution, the resin was washed with DMF (× 3), MeOH (× 3), and CH_2Cl_2 (× 3).

[Step 4: reduction]

The resin obtained in Step 3 was transferred to a 5-mL glass LibraTube® and dried under reduced pressure. After the addition of IPrCuO^{t}Bu (containing an equal amount of NaCl, 11.7 mg, 20.0 μmol, 100 mol%), the vessel was purged with N_2 through evacuation and filling back N_2 three times. Then, a mixture of ^{t}BuOH (190 μL, 2.00 mmol, 100 equiv.), PMHS (168 μL, 2.80 mmol for Si–H, 140 equiv. for Si–H) and toluene (1.0 mL) was added to the vessel. The vessel was shaken continuously at 50 °C for 20 min. The reaction solution was removed, and the resin was washed with THF (× 3), MeOH (× 3), and CH_2Cl_2 (× 3), and dried under reduced pressure.

Step 4 was repeated until no intermediate was observed in off-bead analysis by mass spectrometry.

[Step 5: cleavage and purification]

The resin obtained in Step 4 was transferred to a 6-mL plastic syringe with a filter. The resin was swelled in CH_2Cl_2 for 10 min. To the vessel, 30% HFIP in CH_2Cl_2 (1.0 mL) was added. After continuous shaking for 15 min, the solution was filtrated, and the filtrate was collected. This operation was repeated two times more, and the filtrates were combined. After concentration under reduced pressure, the residue was subjected to silica-gel column chromatography to afford the desired PUFA. The obtained compound was further purified for biological assays by reverse-phase HPLC.

TGFα shedding assay (Fig. 4)

The evaluation of FFAR1 agonistic activity by TGFα shedding assay was performed according to the previously reported procedure with minor modifications.[11,34] In brief, Human embryonic kidney 293 (HEK293) cells transfected with plasmids of AP-TGFα and FFAR1, and were seeded in 96-well plates and incubated at 37 °C (5% CO_2) for 24 h. The cells were stimulated with 3.0 μM PUFA or vehicle in Hank's balanced salt solution (HBSS) for 1 h. After the separation of the conditioned mediums and the

cells, *p*-nitrophenylphosphate (*p*NPP) solution was added into each well. The optical density at 405 nm (OD_{405}) was measured before and after one-hour incubation at room temperature under an ambient atmosphere. AP-TGFα release (%) was calculated according to the following equation: [$\Delta OD_{405,CM}$ / ($\Delta OD_{405,CM}$ + $\Delta OD_{405,Cell}$)], where $\Delta OD_{405,CM}$ and $\Delta OD_{405,Cell}$ denote changes in OD_{405} in the conditioned medium and on the cell surface, respectively, before and after one-hour incubation.

Stability evaluation in mouse liver homogenate (Fig. 5b)

To the solution of 17,18-EpETE (**1e**) or Antiefin (**1r**) (100 μM, 200 μL) in 100 mM phosphate buffer (pH 7.4) was added mouse liver homogenate (20.0 μL) pre-incubated with/without 200 μM sEH inhibitor, TPPU, at 37 °C. After incubation at 37 °C for 0 or 1 h, 50 μL of the mixture was sampled and added with MeCN/H_2O (6:1, 350 μL). The resulting sample was analyzed by LCMS.

Animals

Female wild-type C57BL/6 mice were purchased from Japan SLC (Hamamatsu, Japan) and kept for at least 1 week before experiments in the specific pathogen-free animal facility at the National Institutes of Biomedical Innovation, Health and Nutrition (NIBIOHN; Osaka, Japan). Mice were killed by means of cervical dislocation after achievement of anesthesia with isoflurane (Foranel AbbVie, North Chicago, Ill). All experiments involving mice were conducted in accordance with the guidelines of the Animal Care and Use Committee of NIBIOHN and the Committee on the Ethics of Animal Experiments of NIBIOHN (approval no. DSR01-2R1, DSR04-37R7).

Neutrophil pseudopod formation *in vitro* assay (Figs. 5c and 5d)

The evaluation of inhibitory activity against neutrophil pseudopod formation was performed according to the previously reported procedure with minor modifications.[11,41] In brief, neutrophils were purified

from mouse bone marrow with 65 and 72% Percoll. The neutrophils (4×10^5 cells) were suspended in HBSS containing 0.2% BSA, seeded into fibronectin-coated coverslips (neuVitro, Vancouver, Wash), and incubated at 37 °C (5% CO_2) for 15 min. After treatment with Antiefin (**1r**), 17,18-EpETE (**1e**), or EtOH (vehicle) for 15 min, the cells were then stimulated with 100 nM LTB_4 (Cayman Chemical) for 2 min in 5% CO_2 incubation. The neutrophils were fixed with 4% paraformaldehyde (Nacalai Tesque), permeabilized with 0.5% Triton X-100 (Nacalai Tesque) in Dulbecco's phosphate buffer saline (DPBS), and stained in 100 nM Acti-stain 488 phalloidin (Cytoskeleton, Denver, Colo) for 30 min at room temperature. Cell nuclei were stained by DAPI treatment for 30 min at room temperature, and imaged (model TCS SP8; Leica Microsystems, Wetzlar, Germany).

Contact hypersensitivity *in vivo* experiment (Figs. 5e–h)

The evaluation of anti-inflammatory activity *in vivo* in contact hypersensitivity mouse model was performed as described previously with minor modifications.[11] In brief, the abdominal skin of each mouse was shaved and treated with either 17,18-EpETE (**1e**) (100 or 10 ng in DPBS), Antiefin (**1r**) (100 or 10 ng) or vehicle (50% EtOH in DPBS) by topical application on the abdominal skin. After 30 min, the mice were treated with 25 μL of 0.5% (v/v) DNFB (Nacalai Tesque or Sigma-Aldrich) in a mixture of acetone and olive oil (Nacalai Tesque or Fujifilm-Wako) (4:1). After five days, the mice were treated with the corresponding PUFA or vehicle (with the same dose of the Day 0) by topical application on the ear skin. After 30 min, the fronts and backs of both ears were stimulated with 0.2% (v/v) DNFB (10 μL). After 48 h, ear thickness was measured with a micrometer (model MDC-25MJ 293-230; Mitsutoyo, Kawasaki, Japan).

For neutrophil counting, the skin extracted from the left ears was treated with 3 mg/mL collagenase (Fujifilm-Wako) in RPMI1640 medium (Sigma-Aldrich) containing 2% (v/v) newborn calf serum (Equitech-Bio, Kerrville, Tex) for 90 min at 37 °C with stirring. Cell suspensions were filtered through

cell strainers (pore size, 100 μm; BD Biosciences, Franklin Lakes, NJ) and stained with an anti-CD16/32 mAb (TruStain fcX; BioLegend, San Diego, Calif; 101320; 1:100) to avoid nonspecific staining. Cells were further stained with the following fluorescence-labeled mAbs: fluorescein isothiocyanate (FITC)–anti-Ly6G (BioLegend; 127606; 1:100), allophycocyanin (APC)-Cy7–anti-CD11b (BioLegend; 101226; 1:100) and brilliant violet (BV) 421–anti-CD45 (BioLegend; 103133; 1:100) mAbs. Dead cells were detected by using 7-aminoactinomycin D (7-AAD) (BioLegend; 420404; 1:100) and excluded from analysis. Samples were analyzed by CytoFLEX LX (Beckman Coulter). Data were analyzed with FlowJo 10.10.0 software (TreeStar, Ashland, Ore). Neutrophils were gated as 7-AAD^{-}CD45^{+}Ly6G^{+}CD11b^{+} cells.

Right ear samples were frozen in Tissue-Tek OCT compound (Sakura Finetek, Tokyo, Japan) in liquid nitrogen. Frozen tissue sections (6 μm) were prepared by using cryostat (model CM3050 S, Leica Biosystems, Wetzlar, Germany) and used for hematoxylin and eosin staining.

Statistical analysis

Statistical significance was evaluated using one-way analysis of variance with post-hoc Tukey test for multiple comparison in Prism 10.2.2 software (GraphPad Software, San Diego, CA, USA). Statistical significance was defined as a P value <0.05.

Acknowledgements

This work was performed in part at One-stop Sharing Facility Center for Future Drug Discoveries in Graduate School of Pharmaceutical Sciences, the University of Tokyo.

Funding

This research was supported by JSPS KAKENHI [grant numbers JP22K14780 (to Y.Sai.);

JP22KJ1101 (to M.A.)]; AMED [grant numbers 233fa727001h0002 (to Y.Sai. and J.K.)]; Toyota Riken Scholar Program (to Y.Sai.); Mizuho Foundation for the Promotion of Sciences (to Y.Sai.); KONICA MINOLTA Award in Synthetic Organic Chemistry, Japan (to Y.Sai.); and JST-CREST [grant number JPMJCR21N5 (to S.S.)].

Author contributions

Y.Sai., J.K. and S.S. conceived and designed the project.; Y.Sai., M.A., and Y.San. performed synthetic experiments with the help of J.M. and S.S.; Y.Sai., M.A., A.S., M.H., and T.N. performed cellular experiments with the help of A.U., J.A., J.K. and S.S.; A.S., M.H. and T.N. performed animal experiments with the help of J.K.; and Y.Sai., M.A. and S.S wrote the manuscript, which was edited by all co-authors.

Competing interests

The authors declare the following competing financial interest: the authors (Y.Sai., M.A., Y.San. and S.S.) have filed a patent application (PCT/JP2024/054041). All other authors declare they have no competing interests.

References

1. Dyall, S. C. *et al.* Polyunsaturated fatty acids and fatty acid-derived lipid mediators: Recent advances in the understanding of their biosynthesis, structures, and functions. *Prog. Lipid Res.* **86**, 101165 (2022).
2. Ulven, T. & Christiansen, E. Dietary Fatty Acids and Their Potential for Controlling Metabolic Diseases Through Activation of FFA4/GPR120. *Annu. Rev. Nutr.* **35**, 239–263 (2015).
3. Gorjão, R. *et al.* Comparative effects of DHA and EPA on cell function. *Pharmacol. Ther.* **122**,

56–64 (2009).

4. Isobe, Y. & Arita, M. Identification of novel omega-3 fatty acid-derived bioactive metabolites based on a targeted lipidomics approach. *J. Clin. Biochem. Nutr.* **55**, 79–84 (2014).

5. Leuti, A. *et al.* Bioactive lipids, inflammation and chronic diseases. *Adv. Drug Deliv. Rev.* **159**, 133–169 (2020).

6. Duvall, M. G. & Levy, B. D. DHA- and EPA-derived resolvins, protectins, and maresins in airway inflammation. *Eur. J. Pharmacol.* **785**, 144–155 (2016).

7. Calder, P. C. Polyunsaturated fatty acids and inflammation. *Prostaglandins Leukot. Essent. Fat. Acids* **75**, 197–202 (2006).

8. Ichi, I. *et al.* Identification of genes and pathways involved in the synthesis of Mead acid (20:3n-9), an indicator of essential fatty acid deficiency. *Biochim. Biophys. Acta* **1841**, 204–213 (2014).

9. Harayama, T. & Riezman, H. Understanding the diversity of membrane lipid composition. *Nat. Rev. Mol. Cell Biol.* **19**, 281–296 (2018).

10. Kunisawa, J. *et al.* Dietary ω3 fatty acid exerts anti-allergic effect through the conversion to 17,18-epoxyeicosatetraenoic acid in the gut. *Sci. Rep.* **5**, 9750 (2015).

11. Nagatake, T. *et al.* The 17,18-epoxyeicosatetraenoic acid–G protein–coupled receptor 40 axis ameliorates contact hypersensitivity by inhibiting neutrophil mobility in mice and cynomolgus macaques. *J. Allergy Clin. Immunol.* **142**, 470-484.e12 (2018).

12. Jeffery, T., Gueugnot, S. & Linstrumelle, G. An Efficient Route to Skipped Diynes and Triynes, (Z,Z) Dienes and (Z,Z,Z) Trienes. *Tetrahedron Lett.* **33**, 5757–5760 (1992).

13. Durand, S., Parrain, J. L. & Santelli, M. A Large Scale and Concise Synthesis of γ-Linolenic Acid from 4-Chlorobut-2-yn-1-ol. *Synthesis.* **1998**, 1015–1018 (1998).

14. Proteau-Gagne, A. *et al.* Synthesis and functional pharmacological effects on human bronchi of 20-hydroxyeicosatetraenoic acid. *Chem. Nat. Compd.* **46**, 841–847 (2011).

15. Bräse, S. *Combinatorial Chemistry on Solid Supports* in *Topics in Current Chemistry* (Springer, 2007).

16. Merrifield, R. B. Solid phase peptide synthesis. I. The Synthesis of a Tetrapeptide. *J. Am. Chem. Soc.* **85**, 2149–2154 (1963).

17. Qi, L., Meijler, M. M., Lee, S. H., Sun, C. & Janda, K. D. Solid-phase synthesis of anandamide analogues. *Org. Lett.* **6**, 1673–1675 (2004).

18. Spector, A. A. & Kim, H. Y. Cytochrome P450 epoxygenase pathway of polyunsaturated fatty acid metabolism. *Biochim. Biophys. Acta* **1851**, 356–365 (2015).

19. Mant, C. T. & Hodges, R. S. *High-Performance Liquid Chromatography of Peptides and Proteins*. (CRC Press, 1991).

20. Evano, G. *et al.* Turning unreactive copper acetylides into remarkably powerful and mild alkyne transfer reagents by oxidative umpolung. *Chem. Commun.* **50**, 10008–10018 (2014).

21. Asano, Y., Ito, H., Hara, K. & Sawamura, M. Enantioselective addition of terminal alkynes to aromatic aldehydes catalyzed by copper(I) complexes with wide-bite-angle chiral bisphosphine ligands: Optimization, scope, and mechanistic studies. *Organometallics* **27**, 5984–5996 (2008).

22. Pirrung, M. C., Shuey, S. W., Lever, D. C. & Fallon, L. A convenient procedure for the deprotection of silylated nucleosides and nucleotides using triethylamine trihydrofluoride. *Bioorganic Med. Chem. Lett.* **4**, 1345–1346 (1994).

23. Balas, L., Durand, T., Saha, S., Johnson, I. & Mukhopadhyay, S. Total synthesis of photoactivatable or fluorescent anandamide probes: Novel bioactive compounds with angiogenic activity. *J. Med. Chem.* **52**, 1005–1017 (2009).

24. Whittaker, A. M. & Lalic, G. Monophasic catalytic system for the selective semireduction of alkynes. *Org. Lett.* **15**, 1112–1115 (2013).

25. Isobe, Y. *et al.* Comprehensive analysis of the mouse cytochrome P450 family responsible for

omega-3 epoxidation of eicosapentaenoic acid. *Sci. Rep.* **8**, 7954 (2018).

26. Miyata, N. & Roman, R. J. Role of 20-hydroxyeicosatetraenoic acid (20-HETE) in vascular system. *J. Smooth Muscle Res.* **41**, 175–193 (2005).

27. Tunaru, S. *et al.* 20-HETE promotes glucose-stimulated insulin secretion in an autocrine manner through FFAR1. *Nat. Commun.* **9**, 177 (2018).

28. Hwang, S. H. *et al.* Chemical synthesis and biological evaluation of ω-hydroxy polyunsaturated fatty acids. *Bioorganic Med. Chem. Lett.* **27**, 620–625 (2017).

29. Xu, L. *et al.* Furan fatty acids–Beneficial or harmful to health? *Prog. Lipid Res.* **68**, 119–137 (2017).

30. Christiansen, E. *et al.* Activity of dietary fatty acids on FFA1 and FFA4 and characterisation of pinolenic acid as a dual FFA1/FFA4 agonist with potential effect against metabolic diseases. *Br. J. Nutr.* **113**, 1677–1688 (2015).

31. Khan, M. Z. & He, L. The role of polyunsaturated fatty acids and GPR40 receptor in brain. *Neuropharmacology* **113**, 639–651 (2017).

32. Kimura, I., Ichimura, A., Ohue-Kitano, R. & Igarashi, M. Free fatty acid receptors in health and disease. *Physiol. Rev.* **100**, 171–210 (2020).

33. Defossa, E. & Wagner, M. Recent developments in the discovery of FFA1 receptor agonists as novel oral treatment for type 2 diabetes mellitus. *Bioorg. Med. Chem. Lett.* **24**, 2991–3000 (2014).

34. Inoue, A. *et al.* TGFα shedding shedding assay: an accurate and versatile method for detecting GPCR activation. **9**, 1021–1029 (2012).

35. Houthuijzen, J. M. *et al.* Fatty acid 16:4(n-3) stimulates a GPR120-induced signaling cascade in splenic macrophages to promote chemotherapy resistance. *FASEB J.* **31**, 2195–2209 (2017).

36. Morisseau, C. & Hammock, B. D. Impact of Soluble Epoxide Hydrolase and Epoxyeicosanoids on Human Health. *Annu. Rev. Pharmacol. Toxicol.* **53**, 37–58 (2013).

37. Harris, T. R. & Hammock, B. D. Soluble epoxide hydrolase: Gene structure, expression and deletion. *Gene* **526**, 61–74 (2013).

38. Morisseau, C. *et al.* Relative importance of soluble and microsomal epoxide hydrolases for the hydrolysis of epoxy-fatty acids in human tissues. *Int. J. Mol. Sci.* **22**, 4993 (2021).

39. Rose, T. E. *et al.* 1-Aryl-3-(1-acylpiperidin-4-yl)urea inhibitors of human and murine soluble epoxide hydrolase: Structure-activity relationships, pharmacokinetics, and reduction of inflammatory pain. *J. Med. Chem.* **53**, 7067–7075 (2010).

40. Ostermann, A. I. *et al.* Oral treatment of rodents with soluble epoxide hydrolase inhibitor 1-(1-propanoylpiperidin-4-yl)-3-[4-(trifluoromethoxy)phenyl]urea (TPPU): Resulting drug levels and modulation of oxylipin pattern. *Prostaglandins Other Lipid Mediat.* **121**, 131–137 (2015).

41. Saika, A. *et al.* 17(S),18(R)-epoxyeicosatetraenoic acid generated by cytochrome P450 BM-3 from Bacillus megaterium inhibits the development of contact hypersensitivity via G-protein-coupled receptor 40-mediated neutrophil suppression. *FASEB BioAdvances* **2**, 59–71 (2020).